A microcontact printed nickel passivated copper grid electrode for perovskite photovoltaics

Anjana Wijesekara[1]*,Marc Walker*[2]*, Yisong Han*[2]*, Ross Hatton* [1]***

[1] Department of Chemistry, University of Warwick, CV4 7AL, Coventry, United Kingdom.

[2] Department of Physics, University of Warwick, CV4 7AL, Coventry, United Kingdom.

*Corresponding Author. E-mail: Ross.Hatton@warwick.ac.uk

Abstract

We report a novel transparent copper-based grid electrode fabricated by micro-contact printing, that offers high stability towards oxidation in air. Passivation is achieved using a 2.5 nm thick layer of nickel buried just below the surface of the copper film from which the grid is etched. This approach to electrode passivation retains the advantages associated with using microcontact printing lithography for grid fabrication, of very fast resist deposition and compatibility with the low cost, low toxicity etchant ammonium persulfate. The processes of patterned resist deposition and metal etching is complete within less than 1 minute. Using this approach a grid electrode with far-field transparency of 82% across the wavelength range 300-900 nm and sheet resistance of 6.8 Ohms square is demonstrated, which is shown to be a promising alternative to indium-tin oxide as the transparent electrode in perovskite photovoltaic devices.

Keywords: transparent electrode, copper, microcontact printing, photovoltaic, solar cell, perovskite, metal grid electrode, soft lithography.

Introduction

Transparent conducting electrodes (TCE) serve an indispensable role in a wide range of optoelectronic devices including photovoltaics (PVs)[1], supercapacitors[2], smart windows[3], touch screens[4] and organic light-emitting diodes[5]. Over the past decade a number of innovate approaches have been reported for the fabrication of TCEs based on a fine grid of opaque metal lines together with a high transparency, low conductivity layer that spans the gaps between them.[6-13] This approach to TCE electrode design offers a path to achieving performance matched to the requirements for several potentially very low cost, emerging thin film PVs, including perovskite PVs: A sheet resistance much less than 10 Ohms per square and far-field transparency > 80 % for light wavelengths in the range 400-900 nm.[6–8] Metal mesh electrodes are particularly attractive for organic PVs and perovskite PVs, as a replacement for the transparent conducting oxides (TCOs) indium tin oxide (ITO) and fluorine doped tin oxide (FTO) currently used. This is because ITO uses the high cost element indium, and both of these oxides are inherently brittle which limits their performance on the flexible plastic substrates needed for low-cost roll-to-roll device processing.[9] There is particular interest in ways to produce grid line-widths narrower than 20 microns, which is lower than can be achieved using current industrially relevant processes[10], because this allows for a higher density of grid lines for the same obscured area, reducing the reliance on the layer spanning the gaps between grid lines to conduct charge carriers to the grid. However, for this type of TCE to be truly viable for low cost applications such as perovskite PVs they also need to be fabricated using low cost methods using low toxicity, earth abundant materials.

Methods for the fabrication of metal grid electrodes with very narrow line-width and small line spacing include nano-imprint lithography[11], cracked film lithography[12] and micro-contact printing (μ-CP)[13]. Microcontact printing (μ-CP) is a lithographic method, invented by George M.

Whitesides, that uses a patterned molecular etch resist < 2 nm thick, and can achieve feature sizes as small as 100 nm in copper (Cu), silver (Ag), gold (Au) and aluminum (Al) over large areas.[14] Unlike conventional lithographic techniques, μ-CP is compatible with continuous roll-to-roll processing[15] and because the resist layer is 2-3 orders of magnitude thinner than convention lithographic resists (0.5-5 μm)[16], the amount of solvent needed for the deposition and removal of the resist layer is greatly reduced. Widely available alkyl thiols have proved particularly effective as molecular resists for patterning Au and Cu and can be contact printed onto the metal in a fraction of a second.[17] Despite these advantages there are very few reports pertaining to using this technique to make grid electrodes. To the best of our knowledge, to date there has been only two reports: Xia *et al.*[18] and Bellchambers *et al*.[19] have shown that μ-CP can be used to fabricate Ag grids and Cu grids respectively, the latter on both rigid glass and flexible plastic substrates. The economic case for using Cu instead of Ag is clear-cut, since Cu is < 1% the cost of Ag with comparable electrical conductivity.[20] Unfortunately Cu is more susceptible to oxidation in air, which inevitably ingresses into the device over the long life expected for PV device applications, eroding the conductivity of the electrode. High performance encapsulation is costly, and so its use would inevitably undermine the anticipated cost advantage of perovskite PVs over other types of PV.[21] Consequently there is a need to develop ways to passivate Cu towards oxidation in air without electrically isolating it.

Herein we report a new Cu-based grid electrode fabricated by microcontact lithography that offers high stability towards oxidation in air and demonstrate its utility in model perovskite PV devices as the transparent hole-extracting electrode. Crucially, the fabrication method developed retains the advantages associated with using microcontact lithography: namely very fast resist deposition and compatibility with the low cost, low toxicity, fast etchant ammonium persulfate (APS). The improved stability is achieved using an extremely thin (2.5 nm) nickel layer

buried just below the surface of the Cu electrode, which also serves to inhibit Cu diffusion from the electrode when used as an electrode in PV devices.

Results and discussion

The fabrication process for the novel grid electrode is schematically illustrated in Figure 1 and cross-sectional scanning transmission electron microscopy (STEM) images of the actual electrode are shown in Figure 2. The rationale for the electrode design is as follows: Bulk Ni is resistant to oxidation in air because it forms a compact oxide layer with a self-limiting thickness of < 3 nm.[22] Despite having very similar atomic radii to Cu; Ni 1.62 Å and Cu 1.57 Å, the enthalpy of mixing of Ni with Cu atoms is positive[23] and so these metals do not alloy unless heated to a critical temperature of 627 K (~354^{o}C).[24] For this reason a Ni thickness sufficient to form the native oxide thickness should be capable of passivating an underlying Cu film towards oxidation in air. NiO is also thermodynamically very stable[25] and is a metal-deficient *p*-type semiconductor with an accessible valence band edge for the conduction of holes[26], so its formation in-situ in a PV device would not be expected to electrically isolate the underlying Cu when used as the hole-extracting electrode. Based on the density of Ni and NiO, a 1.76 nm thick Ni film should oxidised in air to form a 3 nm NiO film. Additionally, Ni has an electrical conductivity four times lower than that of Cu and is found to be etched very slowly by the ammonium persulfate (APS)[27] etchant used in this work (Figure S1; Topographic AFM image of the surface of a 5 nm thin Ni metal film before and after etching). APS is the etchant of choice because of its low cost, low environmental toxicity and ease with which it can be recycled.[28] However, when the Ni thickness exceeded 3.5 nm it was difficult to etch to form a well-defined grids. This is attributed to the very slow etching of the top

of the grid lines as compared to fast etching of the sides of the grid lines. For these reasons the optimal thickness was found to be 2.5 nm. The STEM images and associated nano-scale energy dispersive X-ray spectroscopy (EDX) analysis shown in Figure 2 are consistent with the formation of a discrete Ni layer.

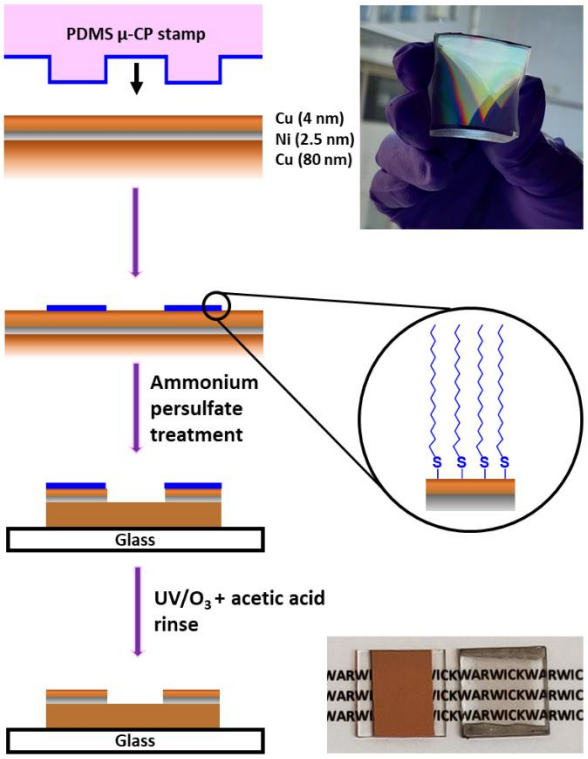

Figure 1: Schematic illustration of the process of fabrication of metal grid electrodes.

The affinity of alkylthiols for Ni metal[29] is much less than that of Cu and so to form a compact HDT monolayer by micro-contact printing a sacrificial Cu layer was deposited on top of the Ni. Importantly, all three metal layers are evaporated sequentially without breaking vacuum. The thickness used for the top Cu layer is 4 nm, which is known to be the minimum thickness of Cu needed to form a continuous layer when thermally evaporated onto a substrate onto which Cu

strongly binds.[30] When the thickness of Cu capping layer was less than 4 nm the reproducibility of the etching process was compromised, likely due to a discontinuous or insufficiently compact HDT monolayer. Metal films are micro-contact printed in ambient air using a polydimethylsiloxane (PDMS) stamp inked with a 0.2 mM hexadecane thiol (HDT) in ethanol: Figure 1. The PDMS stamp is brought into contact with the metal films for ~5 seconds to deposit a compact thiol layer, although much shorter contact times are possible. Metal films patterned with the thiol are immersed in a dilute solution of APS (0.007 mol dm^{-3}) for 30-40 seconds to etch off the unmasked metal. The resulting grid is rinsed with water to remove residual APS, followed by isopropyl alcohol (IPA) to remove the water.

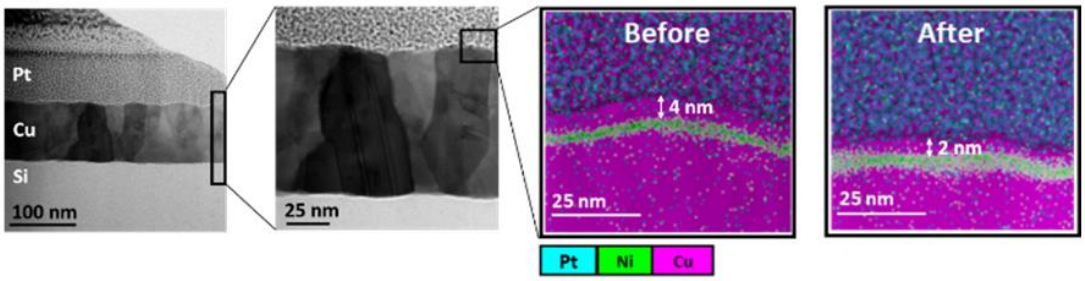

Figure 2: Cross-sectional bright-field STEM images and EDX elemental maps taken from a Cu (80 nm)|Ni (2.5 nm)|Cu(4 nm) planar film. A Pt protection layer is deposited on top of the sample when a TEM lamella is made using a focused ion beam. EDX cross-sections before and after UV-O_3 and acetic acid treatment. Notably, the before and after images do not correspond to the same locations due to the difficulty in returning to the same location.

High-resolution X-ray photoelectron spectroscopy (XPS) analysis of the S 2*p* region of the HDT covered electrode (Figure 3(a)) shows components due to HDT chemisorbed to Cu (labelled Cu-S) and physisorbed HDT (labelled C-S-H). From the ratio of the area under the S $2p_{3/2}$ peaks assigned to these two different sulfur environments it is estimated that ~44% of the HDT monolayer is not actually chemisorbed to the Cu, although this does not undermine its effectiveness as a resist. Figure 3(b) shows the Cu $2p_{3/2}$ region from this sample, showing the absence of a significant quantity of Cu^{2+} states via the lack of shake-up features in the 938 eV – 945 eV range. For application as an electrode in perovskite PV devices the insulating HDT monolayer was removed by brief UV-O_3 treatment. Its removal is evidenced by the reduction in intensity of the C 1*s* peak in the XPS spectrum (Figure S2) and loss of the S 2*p* doublet associated with a thiol linkage to Cu metal: Figure 3 (a) and (c). The majority of the S 2*p* doublet is shifted to higher binding energy consistent with the formation of sulfates.[31] It is evident from the XPS data in Figure 3(b) and 3(d) that UV-O_3 treatment also partially oxidizes the 4 nm thick Cu capping layer. The oxides of Cu are several orders of magnitude less conductive than Cu metal[32] and so they were selectively removed by brief rinsing in glacial acetic acid[33], as evidenced by the disappearance of Cu^{2+} components in Cu $2p_{3/2}$ spectrum: Figure 3(f).

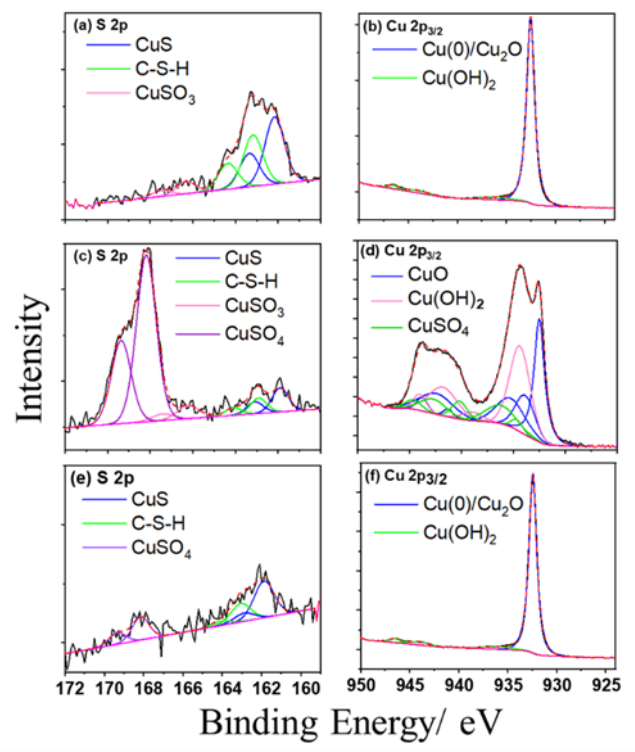

Figure 3: HRXPS spectra of the (a) S 2*p*, (b) Cu 2$p_{3/2}$ for a film of Cu (80 nm)|Ni (2.5 nm)|Cu (4 nm), (c) S 2*p* , (d) Cu 2$p_{3/2}$ for a UV-O_3 treated film of Cu (80 nm)|Ni (2.5 nm)|Cu (4 nm), (e) S 2*p*, (f) Cu 2$p_{3/2}$ for a UV-O_3 and acetic acid treated film of Cu (80 nm)|Ni (2.5 nm)|Cu (4 nm). Key: Solid black line = counts per second (CPS); dashed red line = Total fit.

Cross-sectional STEM image and nanoscale EDX analysis (Figure 2) shows that this process reduces the Cu capping layer thickness from 4 nm to ~2 nm. Upon removal of the Cu oxide layer the Ni 2p peak (Figure S3) becomes much more intense, since it is now buried under a much thinner Cu layer and thus the photoelectron intensity originating from the Ni layer is less attenuated.

Elemental analysis using X-ray fluorescence spectroscopy; Figure S4, confirms that the 2.5 nm Ni layer is not affected by the acetic acid treatment, which is consistent with the TEM/EDX analysis shown in Figure 2, since only the top 2 nm of Cu is removed. This new approach to fabricating passivated Cu grid electrode by μ-CP was used to fabricate grid electrodes with an average total spectral transmittance of over 82.5% ± 2% (across the wavelength range 300-900 nm) and sheet resistance of 6.8 ± 0.7 Ω sq^{-1} (Figure 4). The small variation in transparency and sheet resistance been grid electrodes fabricated in the same way is attributed to very small variations in the widths of the grid lines; 1.85 ± 0.1 μm, that results from the inevitable variation in the applied pressure during the PDMS stamping step, which is performed by hand. The Haacke figure-of-merit (Transmittance[10] / sheet resistance)[34] - a metric commonly used to compare the performance of different types of transparent electrodes is 0.021, which is comparable to commercial ITO glass (0.024)[19] when the average transparency over the wavelength range 400-800 nm is used rather than the transparency at 550 nm only. SEM imaging of the grids together with AFM imaging shows that the grid-lines are well-defined with a line-width of 1.85 ± 0.1 μm and total metal thickness of 86.5 nm (Figure 4).

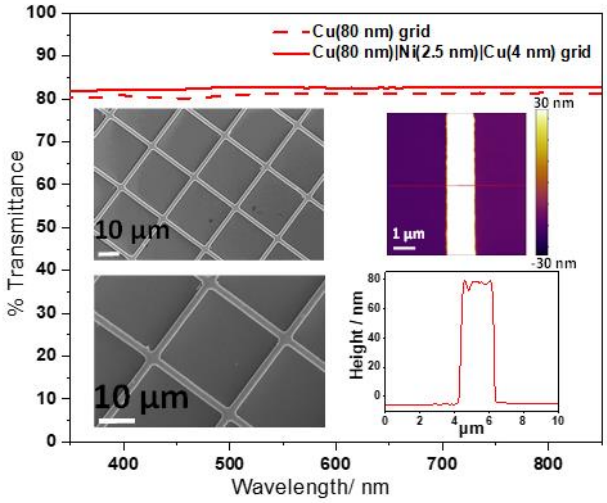

Figure 4: Total far-field transparency of grid electrodes. Inset: SEM images of typical grid electrodes and corresponding AFM image of part of a Cu (80 nm)|Ni (2.5 nm)|Cu (4 nm) grid-line together with a representative cross-section.

Electrode stability testing

The rate of oxidation of grid electrodes with and without Ni passivation layer at ambient temperature (~20^{o}C) and relative humidity (30-40%), was extremely slow with no measurable deterioration in sheet resistance after 4.5 months: Figure 5 (a). To accelerate the process of oxidation the grids were annealed at 85 ^{o}C and relative humidity (30 %-40 %). After 20 hours the sheet resistance of grids with and without a 2.5 nm Ni layer had increased by 5 % and 22 % respectively, which evidences the passivation effect of the 2.5 nm Ni layer for the Cu grid. However, this test does not capture the true extent to which the 2.5 nm Ni layer passivates Cu, since oxidation of the grids occurs both from the top surface and the side of the grid lines and Ni is not present on the sidewalls of the grids after µ-CP. Whilst the sidewalls of the grid lines

constitute only a small fraction of the total surface area of the grid electrode it is likely that oxidation of the sidewalls contributes disproportionality to the measured increase in sheet resistance in the case of the grid with the Ni layer. To determine the effectiveness of the Ni passivation layer without this added complexity, the resistance of unpatterned optically thin Cu films (with and without a Ni passivation layer) heated in air at 85^{o}C was monitored as a function of time. For both cases the same total metal thickness of 21.5 nm was used, and films were deposited onto mixed molecular adhesive treated glass to ensure a compact slab-like film, and UV-O_3 and acetic acid treated according to the same procedure as used for metal grid fabrication. A metal film thickness much less than used for the grids was used for this experiment so that a significant percentage change in resistance occurs over a shorter timeframe. After an initial decrease in sheet resistance over the first ~1.5 hrs (Figure 5 (d)) the sheet resistance of the Ni passivated film increases linearly with time. The time taken for the sheet resistance of the Ni passivated film to increase by 50 % from its lowest point is 34 hrs, which compares to 17 minutes for a Cu film without Ni passivation: a 120-fold decrease in the rate of oxidation. Notably, an initial small decrease in sheet resistance is common for the Ni passivated grid electrodes but is much more pronounced in optically thin films. The reason for this initial improvement in conductance is tentatively attributed to the relaxation of the Cu lattice after deposition because Cu atoms are known to be mobile at room temperature[33], improving the electrical contact between adjacent crystallites.

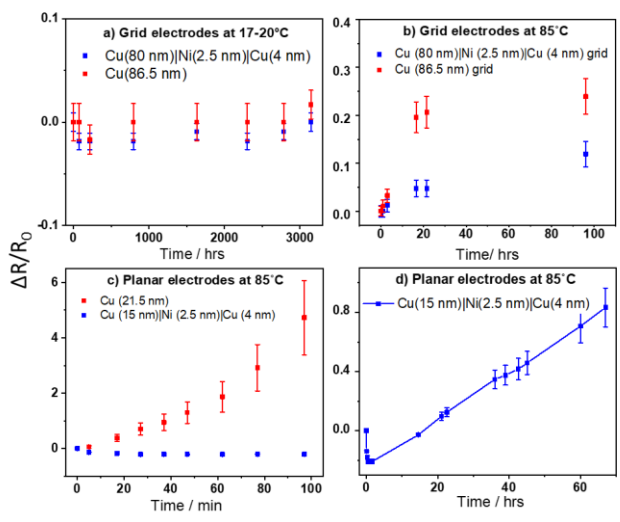

Figure 5: Plots of relative change in sheet resistance with time; a) Grid electrodes (80 nm) in air at room temperature, b) Grid electrodes (80 nm) annealed at 85 ˚C in air, c) Planar electrodes (21.5 nm) annealed at 85 ˚C in air and d) Cu (15 nm)| Ni (2.5 nm)| Cu (4 nm) planar electrode annealed at 85 ˚C in air. All electrodes were UV-O_3 treated and acetic acid rinsed according to the procedure used for grid fabrication.

Notably, Stewart *et al.*[35] reported the sheet resistance of Cu nanowires chemically plated with 18 nm of Ni and annealed at 85 ˚C at 80 % relative humidity remained unchanged after 24 hours. Whilst the humidity during our test was lower (and so the test condition less aggressive) it is notable that grids are remarkably stable given that the Ni passivation layer is a factor of ~7 thinner than that used to passivate the Cu nanowires. We have previously shown that a 0.8 nm aluminum layer deposited by vacuum evaporation onto Cu is remarkably effective at passivating Cu films towards oxidation in air because the oxide plugs the grain boundaries between the Cu

crystallites, which are that part of the film most susceptible to oxidation.[36] It its tentatively suggested that the same mechanism is operative here, with the added benefit that the Ni layer is continuous and forms a self-limiting passivating oxide.

To make these grid electrodes suitable for use as the transparent electrode in perovskite PVs the gaps between grid lines needs to be spanned by the conductive polymer poly(3,4-ethylenedioxythiophene)-poly(styrenesulfonate) (PEDOT:PSS). For this purpose, we have used the highly conductive formulation PH1000 (Heraeus Clevios™). PEDOT:PSS is processed from aqueous solution and its acidity makes it poorly compatible with most metals.[37] Additionally PEDOT:PSS is dissolved by polar solvents such as those used for the deposition of perovskite films (e.g. dimethyl sulfoxide (DMSO) and dimethylformamide (DMF)). To circumvent these issues we have added 0.5 wt% imidazole to neutralize the free PSS[38] and 1 wt% (3-glycidyloxypropyl)trimethoxysilane (GOPS) to cross-link the film via an epoxy ring opening reaction of GOPS which allows binding of GOPS to sulphonate groups in PSS and siloxane cross linking.[39] To our knowledge this combination of additives for PEDOT:PSS has not been reported before. The inclusion of these additives resulted in no significant change in surface roughness: Figure S5. The sheet resistance increased from 1.2 kΩ / sq to 14.5 MΩ / sq upon inclusion of imidazole and GOPS, but this increase was reversed upon addition of 5 wt. % DMSO. The work function of the PH1000 blend and the pristine PH1000 measured using a Kelvin probe is 4.36 ± 0.01 eV and 4.99 ± 0.01 eV respectively. The decrease in the work function is due to the addition of GOPS and renders the electrode work function too low for efficient hole-extraction in perovskite PVs. It was therefore necessary to deposit a thin film of the high work function PEDOT:PSS formulation; Al 4083 (Heraeus Clevios™) on top of the blend to increase the work function to

4.94 eV. Grid electrodes coated with PH1000 blend with and without a passivating Ni layer showed a high degree of stability with ≤ 3 % increase in resistance after 1600 hrs in air.

Perovskite PV devices

To demonstrate the application of this electrode in perovskite PVs, model tin perovskite PV devices were fabricated with the architecture Cu (80 nm)|Ni (2.5 nm)|Cu (4 nm) grid| PH1000 blend| Al 4083 | $FA_{0.8}GA_{0.2}SnI_3$+1 % $EDAI_2$ + 10 % SnF_2[40]| C_{60}|BCP|Ag. These devices were tested under one sun simulated solar illumination, and device stability was tested under load at the maximum power-point.

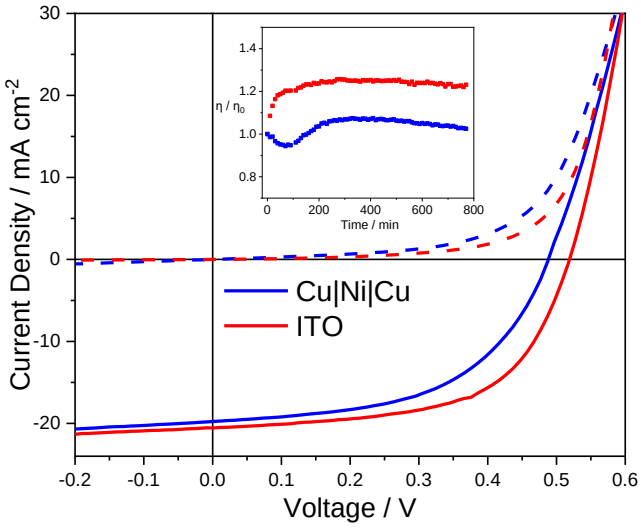

Figure 6: Typical current-voltage characteristic for device with the structure: Transparent electrode the structure | PEDOT:PSS (Al 4083)| Perovskite | C_{60}| BCP |Ag (where the transparent electrode = ITO glass or Cu | Ni | Cu (grid) | PEDOT:PSS (PH 1000)), in the dark (dotted lines) and under 1 sun simulated solar illumination (solid lines). Inset: Evolution of the efficiency of

perovskite PV device under constant 1 sun simulated illumination and load (maximum power point). Testing performed in a nitrogen-filled glove box (≤1 ppm water and oxygen).

Figure 6 shows that the short-circuit current density (J_{sc}) is comparable for devices with grid electrodes (19.76 ± 2.13 mA cm^{-2}) and an ITO electrode (20.53 ± 2.86 mA cm^{-2}). However, the fill-factor (*FF*) and V_{oc} are lower in the former (*FF*: 0.55 ± 0.04, 0.60 ± 0.04 and V_{oc}: 0.49 ± 0.03 V, 0.52 ± 0.04 V). PEDOT:PSS with imidazole and GOPS cross-linker has a conductivity equal to that of PEDOT:PSS (PH 1000), which at the thickness used here (70 nm) is more than sufficient to span the 27.2 micron gaps between Cu grid lines without degrading device fill-factor[19] and so the lower *FF* and V_{oc} are not due parasitic resistance associated with the layer spanning the gaps between grid lines. It is evident from the dark current characteristic, in Figure 6, that the current leakage across the device results from the earlier onset of forward injection. AFM analysis (Figure S6) shows that PEDOT:PSS forms a conformal layer on top of the grid, but the perovskite film does not, so the perovskite is locally thinner above the grid lines. The lower *FF* in devices using a Cu grid electrode is therefore attributed to the fact that perovskite layer is not of uniform thickness, with a higher electric field and lower shunt resistance in that part of the device above the grid lines. It is reasonable to expect that the likelihood of filamentary shunts increases with decreasing perovskite thickness. The development of a planarizing hole-transport layer is the logical solution to this problem, although this is beyond the scope of the current study. Notability however, even though there is a variation in the perovskite thickness across the grid lines, the devices are stable when tested under 1 sun simulated illumination under nitrogen under load at the maximum power point: Figure 6 inset and Figure S7, which bodes well for the likely stability of a device with a planarized hole-transport layer.

Conclusions

In summary, we have demonstrated a novel approach to fabricate Ni passivated Cu grid transparent grid electrodes using micro-contact printing that retains the advantages of using an alkyl thiol resist (fast deposition) and compatibility with the low toxicity etchant APS. We have used this approach to fabricate electrodes based on a nickel passivated copper grid and conducting polymer overlayer suitable for use as the transparent electrode in perovskite PV devices. Whilst there is considerable scope for further optimization of the grid design (i.e. line-width and pitch) and charge transport layer design (i.e. development of a suitable planarization layer) this work points the way to achieving the very challenging goal of a high performance, low cost, truly environmentally sustainable transparent electrode matched to the needs of emerging thin film PVs, of which perovskite PVs are but one.

Experimental methods

Substrate cleaning

Substrates were cleaned by ultrasonic agitation in a dilution solution of surfactant followed by deionized water, acetone and IPA for 15 minutes each. Substrates were dried using a stream of nitrogen and were UV-O_3 treated for 15 minutes immediately before use.

Electrode fabrication

An 80 nm layer of Cu was deposited by thermal evaporation of Cu pellets at a rate of 1.2-1.5 Å s^{-1} followed by a 2.5 nm of Ni at a rate of 1 Å s^{-1} and 4 nm of Cu at a rate of 1 Å s^{-1}. All the metal layers were deposited under the same vacuum (2×10^{-6} mbar). All the evaporations were performed using an MBRAUN bell-jar evaporator system located inside a N_2 filled glove box (MBRAUN

MB 20G LMF). The metal films were microcontact printed in ambient air using a PDMS stamp (line-width = 1.4 μm and pitch = 27.2 μm) inked with 0.2 mM HDT solution in ethanol. Details of the PDMS stamp fabrication are given in reference 19 of this paper. In summary, a mixture of PDMS : crosslinker (10:1) (SYLGARD 184 silicone elastomer kit) was poured onto the master with 1.4 μm wide lines and 10% metal coverage and left to cure in a drying oven at 70^{o} C overnight. The PDMS stamp was fully covered with few drops of 0.2 mM HDT and the ink was left on the stamp for 20 seconds to allow the solvent to permeate into the stamp, followed by blowing with N_2 for one minute to blow off excess liquid and to dry the stamp surface. Stamps were brought into contact with the metal film for less than ~5 seconds to deposit a compact thiol layer. Then the patterned metal films were immersed in a dilute solution of ammonium persulphate (0.007 mol dm^{-3}) for 30-40 seconds to etch off the unmasked Cu. The resulting electrode was washed with deionized water followed by IPA to remove any residual APS. The HDT mask was finally removed by a 15-minute UV-O_3 treatment followed by an acetic acid wash to selectively remove any oxides of Cu.

Stability studies

Substrates were prepared by evaporating 15 nm of Cu followed by 2.5 nm Ni and 4 nm of Cu onto a glass substrate with MPTMS:APTMS mixed monolayer under the same vacuum. A Cu film of 21.5 nm deposited onto a glass substrate with MPTMS:APTMS mixed monolayer was used as the control for this annealing study. All the electrodes were subjected to a 15-minute UV-O_3 treatment followed by an acetic acid wash. Electrodes were placed on hotplate at 85 ˚C and the resistance was measured at regular intervals. The number of identical samples of each type was 4, and the sheet resistance was measured using the 2-point probe method. Electrical contact was made using two parallel strips of sliver along the full length of rectangular samples. The distance between the

parallel silver electrodes was measured using a caliper. For the thermal stability measurements, the temperature of the hotplate was monitored continuously using a programmable temperature probe.

Electronic absorption spectroscopy

Far-field transmittance of metal films on glass were measured over the wavelength range of 350-850 nm using 150 mm Spectral on Integrating Sphere coupled to PerkinElmer LAMBDA high performance series of UV/vis spectrometer. The incident beam passed through the substrate first.

Scanning transmission electron microscopy (STEM)

Cross-sectional TEM specimens were prepared using a focused ion beam. The specimens were observed and analysed in a JEOL ARM 2000F TEM, equipped with a 100 mm^2 Oxford Instruments windowless EDX detector.

X-ray photoelectron spectroscopy (XPS)

XPS analysis was performed using a Kratos AXIS Ultra DLD. Samples were unavoidably exposed to air for approximately 1 min during transfer from an air-tight box to the vacuum chamber of the instrument. XPS measurements were carried out in an ultrahigh vacuum system with a base pressure of $5x10^{-11}$ mbar. The sample was excited with X-rays from a monochromated Al Kα source ($h\nu = 1{,}486.7$ eV), with the photoelectrons being detected at a 90° take-off angle. The sputtering was carried out at room temperature using a Mini beam I ion gun (Kratos Analytical). A beam of 4 keV Ar+ ions was incident on a 3 × 3 mm area of the sample surface. Curve fitting was performed using the Casa XPS package, incorporating Voigt (mixed Gaussian Lorentzian)

line shapes and a Shirley background. The oxidation states of the Cu were analysed using the work of Biesinger [41] as a guide.

Atomic force microscopy (AFM)

AFM imaging was performed in tapping mode using an Asylum Research MFP – 3D to determine the step height of the films and morphologies.

Scanning electron microscopy (SEM)

SEM imaging was performed using a Zeiss SUPRA 55VP field emission gun SEM.

Device fabrication

The PEDOT:PSS PH1000 was deposited by dropping onto the ITO or grid electrode so as to cover the entire substrate, then spun at 5000 rpm for 60 seconds in ambient air followed by a 10 minute annealing at 120˚C. The PEDOT:PSS Al 4083 was then deposited by dropping onto the PH1000 coated substrate so as to cover the entire substrate, then spun at 5000 rpm for 60 seconds in ambient air followed by a 10 minute annealing at 120˚C. These electrodes were transferred to a nitrogen filled glovebox ($\leq$ 1 ppm O_2 and H_2O) and a solution of $FA_{0.78}GA_{0.2}SnI_3$+1 wt% $EDAI_2$+10 mol% SnF_2 from DMSO was spin coated at 5000 rpm for 90 seconds to the electrodes coated with PEDOT:PSS. Chlorobenzene (600 µL) was dropped after 35 seconds during the spin coating. The resulting perovskite film was annealed at 70˚C for 15 minutes to remove any residual DMSO. Then a 32.5 nm of C_{60} was deposited by thermal evaporation at a rate of 0.1-0.4 Å s^{-1}. The device was completed by deposition of 5 nm BCP at 0.6-0.7 Å s^{-1} followed by 100 nm of Ag at 1-1.5 Å s^{-1}. Thermal evaporations were performed at a pressure of 2×10^{-6} mbar with substrate rotation.

The Ag electrode was deposited through a shadow mask to make six devices per slide, each with an area of 6 mm^2.

Device testing

Device testing was performed in the same nitrogen filled glove box as used for device fabrication ($\leq$ 1 ppm O_2 and H_2O) using an ABET Technologies Sun 2000 solar simulator. Current density–voltage (J–V) curves were measured using a Keithley 2400 source-meter under AM1.5 G solar illumination at 100 mW cm^{-2} (1 sun), scanned from -0.2 V to + 1 V at 0.1 Vs^{-1}. *J-V* measurements were made using custom LabVIEW program. Stability tests were performed under continuous 1 sun simulated solar illumination (Xenon short arc lamp, AM1.5 G solar illumination at 100 mW cm^{-2}) with the device under load at, or very close to, maximum power point. During device testing the temperature of the device increases to ~43^{o}C.

Supporting Information

All data supporting this study are provided as supplementary information accompanying this paper.

Description: Additional, AFM, XPS, X-ray fluorescence (elemental analysis) and photovoltaic device stability data.

Author Contributions

The manuscript was written through contributions of all authors. All authors have given approval to the final version of the manuscript.

Funding Sources

The authors would like to thank the United Kingdom Engineering and Physical Sciences Research Council (EPSRC) for funding (Grant numbers: EP/N009096/1) and the University of Warwick for the award of a Chancellor's International Scholarship to Anjana Wijesekara.

References

(1) Park, J. H.; Lee, D. Y.; Kim, Y. H.; Kim, J. K.; Lee, J. H.; Park, J. H.; Lee, T. W.; Cho, J. H. Flexible and Transparent Metallic Grid Electrodes Prepared by Evaporative Assembly. *ACS Appl. Mater. Interfaces* **2014**, *6* (15), 12380–12387.

(2) Zhang, C. (John); Nicolosi, V. Graphene and MXene-Based Transparent Conductive Electrodes and Supercapacitors. Energy Storage Mater. **2019**, *16* (May 2018), 102–125.

(3) Mallikarjuna, K.; Kim, H. Highly Transparent Conductive Reduced Graphene Oxide/Silver Nanowires/Silver Grid Electrodes for Low-Voltage Electrochromic Smart Windows. *ACS Appl. Mater. Interfaces* **2019**, *11* (2), 1969–1978.

(4) Kim-Lee, H. J.; Hong, S. W.; Kim, D. K.; Kim, J.; Kim, H. S.; Chung, S. W.; Cho, E. H.; Kim, H. S.; Lee, B. K. On-Screen Fingerprint Sensor with Optically and Electrically Tailored Transparent Electrode Patterns for Use on High-Resolution Mobile Displays. *Microsystems Nanoeng.* **2020**, *6* (1), 98.

(5) Naka, S. Transparent Electrodes for Organic Light-Emitting Diodes. *Transparent Conduct. Mater.* **2018**, 301–315.

(6) Lee, H. B.; Jin, W. Y.; Ovhal, M. M.; Kumar, N.; Kang, J. W. Flexible Transparent Conducting Electrodes Based on Metal Meshes for Organic Optoelectronic Device

Applications: A Review. J. Mater. Chem. C **2019**, 7 (5), 1087–1110.

(7) Jacobs, D. A.; Catchpole, K. R.; Beck, F. J.; White, T. P. A Re-Evaluation of Transparent Conductor Requirements for Thin-Film Solar Cells. *J. Mater. Chem. A* **2016**, *4* (12), 4490–4496.

(8) Rowell, M. W.; McGehee, M. D. Transparent Electrode Requirements for Thin Film Solar Cell Modules. *Energy Environ. Sci.* **2011**, *4* (1), 131–134.

(9) Yun, J. Ultrathin Metal Films for Transparent Electrodes of Flexible Optoelectronic Devices. *Advanced Functional Materials*. **2017**, 27, 1606641.

(10) Zhou, H.; Song, Y. Fabrication of Silver Mesh/Grid and Its Applications in Electronics. *ACS Appl. Mater. Interfaces* **2021**, 13 (3), 3493-3511.

(11) Xu, K.; Yang, M.; Zhou, Y.; Wang, L. Metal Mesh Electrode Array Fabricated by Plate-to-Roll Nanoimprint Lithography. *SN Appl. Sci.* **2020**, *2* (2), 1–8.

(12) Muzzillo, C. P.; Reese, M. O.; Mansfield, L. M. Fundamentals of Using Cracked Film Lithography to Pattern Transparent Conductive Metal Grids for Photovoltaics. *Langmuir* **2020**, *36* (17), 4630–4636.

(13) Zou, J.; Yip, H. L.; Hau, S. K.; Jen, A. K. Y. Metal Grid/Conducting Polymer Hybrid Transparent Electrode for Inverted Polymer Solar Cells. *Appl. Phys. Lett.* **2010**, *96* (20), 203301-203301-3.

(14) Zhao, X. M. Soft Lithographic Methods for Nano-Fabrication. *J. Mater. Chem.* **1997**, *7* (7), 1069–1074.

(15) Hizir, F. E.; Hale, M. R.; Hardt, D. E. Manufacturing Conductive Patterns on Polymeric Substrates: Development of a Microcontact Printing Process. *J. Micromechanics Microengineering* **2020**, *30* (11), 115008-115023.

(16) Sam, F. L. M.; Mills, C. A.; Rozanski, L. J.; Silva, S. R. P. Thin Film Hexagonal Gold Grids as Transparent Conducting Electrodes in Organic Light Emitting Diodes. *Laser Photonics Rev.* **2014**, *8* (1), 172–179.

(17) Kumar, A.; Whitesides, G. M. Features of Gold Having Micrometer to Centimeter Dimensions Can Be Formed through a Combination of Stamping with an Elastomeric Stamp and an Alkanethiol "Ink" Followed by Chemical Etching. *Appl. Phys. Lett.* **1993**, *63* (14), 2002-2004.

(18) Xia, Y.; Kim, E.; Whitesides, G. M. Microcontact Printing of Alkanethiols on Silver and Its Application in Microfabrication. *J. Electrochem. Soc.* **1996**, *143* (3), 1070–1079.

(19) Bellchambers, P.; Varagnolo, S.; Maltby, C.; Hatton, R. A. High-Performance Transparent Copper Grid Electrodes Fabricated by Microcontact Lithography for Organic Photovoltaics. *ACS Appl. Energy Mater.* **2021**, *4*, 4150–4155.

(20) West, P. R.; Ishii, S.; Naik, G. V.; Emani, N. K.; Shalaev, V. M.; Boltasseva, A. Searching for Better Plasmonic Materials. *Laser Photonics Rev.* **2010**, *4* (6), 795–808.

(21) Corsini, F.; Griffini, G. Recent Progress in Encapsulation Strategies to Enhance the Stability of Organometal Halide Perovskite Solar Cells. *J. Phys. Energy* **2020**, *2* (3), 031002-031029.

(22) Unutulmazsoy, Y.; Merkle, R.; Fischer, D.; Mannhart, J.; Maier, J. The Oxidation Kinetics of Thin Nickel Films between 250 and 500 °c. *Phys. Chem. Chem. Phys.* **2017**, *19* (13),

9045–9052.

(23) Srikanth, S.; Jacob, K. T. Thermodynamic Properties of Cu–Ni Alloys: Measurements and Assessment. *Mater. Sci. Technol. (United Kingdom)* **1989**, *5* (5), 427–434.

(24) Ni (Nickel) Binary Alloy Phase Diagrams. In *Alloy Phase Diagrams*; Okamoto, H., Schlesinger, M. E., Mueller, E. M., Eds; ASM International, **2018**, 3, 520–533.

(25) Haugsrud, R. On the High-Temperature Oxidation of Nickel. *Corros. Sci.* **2003**, *45* (1), 211–235.

(26) Jagadamma, L. K.; Blaszczyk, O.; Sajjad, M. T.; Ruseckas, A.; Samuel, I. D. W. Efficient Indoor P-i-n Hybrid Perovskite Solar Cells Using Low Temperature Solution Processed NiO as Hole Extraction Layers. *Sol. Energy Mater. Sol. Cells* **2019**, *201* (August), 110071-110081.

(27) Turrentine, J. W. Action of Ammonium Persulphate on Metals. *J. Phys. Chem.* **1907**, *11* (8), 623–631.

(28) Alzate, A.; López, M. E.; Serna, C. Recovery of Gold from Waste Electrical and Electronic Equipment (WEEE) Using Ammonium Persulfate. *Waste Manag.* **2016**, *57*, 113–120.

(29) Porto, T. V.; Wilson, M. T.; Worrall, J. A. R. Copper and Nickel Bind via Two Distinct Kinetic Mechanisms to a CsoR Metalloregulator. *Dalt. Trans.* **2015**, *44* (46), 20176–20185.

(30) Bellchambers, P.; Walker, M.; Huband, S.; Dirvanauskas, A.; Hatton, R. A. Enhanced Oxidation Stability of Transparent Copper Films Using a Hybrid Organic-Inorganic Nucleation Layer. *ChemNanoMat* **2019**, *5* (5), 619–624.

(31) Watanabe, M.; Ando, H.; Handa, T.; Ichino, T.; Kuwaki, N. Comparative XPS Study of Silver and Copper Surfaces Exposed to Flowing Air Containing Low Concentration of Sulfur Dioxide. *Zairyo-to-Kankyo* **2007**, 56(1), 10-15.

(32) Liu, M. S.; Lin, M. C. C.; Wang, C. C. Enhancements of Thermal Conductivities with Cu, CuO, and Carbon Nanotube Nanofluids and Application of MWNT/Water Nanofluid on a Water Chiller System. *Nanoscale Res. Lett.* **2011**, *6* (1):297.

(33) Chavez, K. L.; Hess, D. W. A Novel Method of Etching Copper Oxide Using Acetic Acid. *J. Electrochem. Soc.* **2001**, *148* (11), G640-G643

(34) Haacke, G. New Figure of Merit for Transparent Conductors. *J. Appl. Phys.* **1976**, *47* (9), 4086–4089.

(35) Stewart, I. E.; Rathmell, A. R.; Yan, L.; Ye, S.; Flowers, P. F.; You, W.; Wiley, B. J. Solution-Processed Copper-Nickel Nanowire Anodes for Organic Solar Cells. *Nanoscale* **2014**, *6* (11), 5980-5988.

(36) Bellchambers, P.; Lee, J.; Varagnolo, S.; Amari, H.; Walker, M.; Hatton, R. A. Elucidating the Exceptional Passivation Effect of 0.8 Nm Evaporated Aluminium on Transparent Copper Films. *Front. Mater.* **2018**, 5 (71),

(37) Cameron, J.; Skabara, P. J. The Damaging Effects of the Acidity in PEDOT:PSS on Semiconductor Device Performance and Solutions Based on Non-Acidic Alternatives. **2020**, *7*, 1759-1772.

(38) Wang, Q.; Chueh, C. C.; Eslamian, M.; Jen, A. K. Y. Modulation of PEDOT:PSS PH for Efficient Inverted Perovskite Solar Cells with Reduced Potential Loss and Enhanced

Stability. *ACS Appl. Mater. Interfaces* **2016**, *8* (46), 32068–32076.

(39) Håkansson, A.; Han, S.; Wang, S.; Lu, J.; Braun, S.; Fahlman, M.; Berggren, M.; Crispin, X.; Fabiano, S. Effect of (3-Glycidyloxypropyl)Trimethoxysilane (GOPS) on the Electrical Properties of PEDOT:PSS Films. *J. Polym. Sci. Part B Polym. Phys.* **2017**, *55* (10), 814–820.

(40) Jokar, E.; Chien, C. H.; Tsai, C. M.; Fathi, A.; Diau, E. W. G. Robust Tin-Based Perovskite Solar Cells with Hybrid Organic Cations to Attain Efficiency Approaching 10%. *Adv. Mater.* **2019**, *31* (2), 1–7.

(41) Biesinger, M. C. Advanced Analysis of Copper X-Ray Photoelectron Spectra. *Surf. Interface Anal.* **2017**, *49* (13), 1325–1334.

ToC Graphic

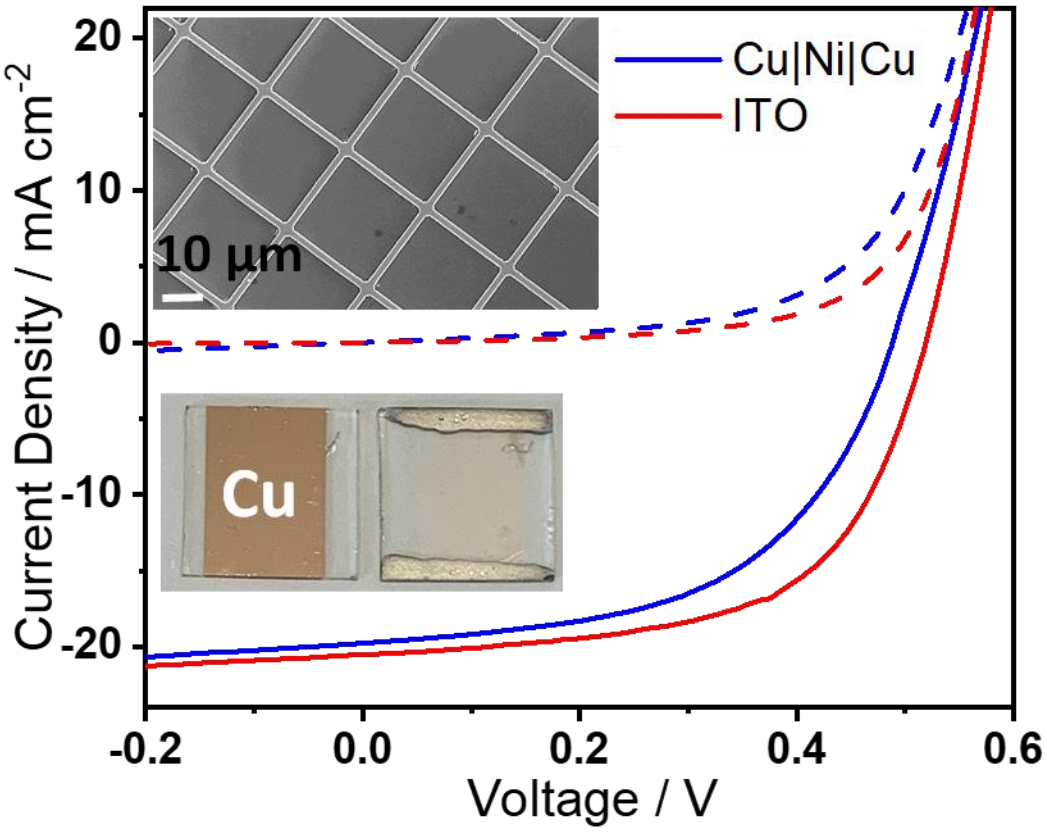
Current Density / mA cm-2
Voltage / V
Cu|Ni|Cu
ITO
10 µm
Cu
20
10
0
-10
-20
-0.2
0.0
0.2
0.4
0.6